A Dielectric Model of Human Breast Tissue in Terahertz Regime

Bao C. Q. Truong, *Student Member, IEEE*, Hoang D. Tuan*, *Member, IEEE*, Anthony J. Fitzgerald, Vincent P. Wallace, *Member, IEEE*, and Hung T. Nguyen, *Senior Member, IEEE*

Abstract—The double Debye model has been used to understand the dielectric response of different types of biological tissues at terahertz (THz) frequencies but fails in accurately simulating human breast tissue. This leads to limited knowledge about the structure, dynamics, and macroscopic behavior of breast tissue, and hence, constrains the potential of THz imaging in breast cancer detection. The first goal of this paper is to propose a new dielectric model capable of mimicking the spectra of human breast tissue's complex permittivity in THz regime. Namely, a non-Debye relaxation model is combined with a single Debye model to produce a mixture model of human breast tissue. A sampling gradient algorithm of nonsmooth optimization is applied to locate the optimal fitting solution. Samples of healthy breast tissue and breast tumor are used in the simulation to evaluate the effectiveness of the proposed model. Our simulation demonstrates exceptional fitting quality in all cases. The second goal is to confirm the potential of using the parameters of the proposed dielectric model to distinguish breast tumor from healthy breast tissue, especially fibrous tissue. Statistical measures are employed to analyze the discrimination capability of the model parameters while support vector machines are applied to assess the possibility of using the combinations of these parameters for higher classification accuracy. The obtained analysis confirms the classification potential of these features.

Index Terms—Classification, dielectric properties, optimization, statistical analysis, support vector machine (SVM), terahertz (THz).

I. INTRODUCTION

RECENT developments in broadband-pulse generation of terahertz (THz) radiation and its detection has accelerated biomedical applications in this frequency range. The THz imaging has now emerged as a potential medical imaging technique to identify contrast between various types of tissue [1]–[3]. Its advances are based on the nature of THz radiation. Having longer wavelengths than those in visible/near-infrared domain, THz waves propagate inside biological tissues with less scattering. Significantly low power levels of THz radiation in typical time-domain systems satisfy the recommended safety threshold for the human body [4]. Another distinct asset is the high sensitivity of THz to water/high water-content materials, making THz imaging a feasible tool for cancer detection [5]. The high absorption of THz radiation by water is considered as a dominant agent producing visible contrast features in THz images between normal and cancerous tissues due to the higher water content of tumor in comparison to normal tissue [6]. Protein, RNA, and DNA content are postulated to affect the interaction of THz radiation with tissue, along with water, and hence, present themselves as potential sources of contrast [2], [7].

The THz images showing contrast between healthy breast tissues and tumors in previous studies show the potential of the imaging technique for accurately detecting the margins of cancer in breast conserving surgery (BCS) [2], [3]. While the increase in absorption and refractive index of breast tumor compared with healthy tissue can explain the contrast in THz images, their root causes still require more thorough studies to be explicated [8]. Apart from this, a solid understanding of the contrast mechanism also has a positive impact on determining essential features for more accurate classification, and hence, more precise cancer-margin detection in BCS. In fact, modeling dielectric properties plays a vital role not only in explaining the distinct features between healthy tissue and tumor in THz images, but also in providing potential parameters for tissue pathology diagnosis and cancer detection and improved diagnostic instrumentation.

The dielectric model can offer a theoretical framework characterizing the complex permittivity of tissue, which reflects interactions between molecules and the THz radiation [7]. For instance, the complex permittivity of human skin in the THz regime can be described by the double-Debye model, which combines the slow and fast relaxation processes of water molecules [9]. This dielectric function was initially used for polar liquid, especially water, and its application for human skin is supported by the fact that skin contains a large proportion of water. However, the free water content of other human body parts may be considerably less than that of skin, which means that the dielectric responses of those tissues may not comply with the simple Debye relaxations. Alternatively, the so-called biological water, or hydration water, which is constructed by chains of protein and their surrounding water molecules, with its increasing content is likely to cause non-Debye responses in dielectric spectra of tissue [10]. Indeed, the double-Debye model fails to obtain a requisite fit for complex permittivity of breast tissue due to an increase observed in the real part of complex permittivity spectra of human breast in the range below 1 THz [8]. The heterogeneity of breast tissue may form more

complex molecular chains affecting the dielectric response. A suitable permittivity model for breast in THz regime is yet to be achieved in the literature. The first aim of our study is to propose a new mixture dielectric model, which not only provides an excellent fit to the complex permittivity of both healthy and cancerous breast tissue but also facilitate a deeper insight into the contrast mechanism at a molecular level. Second, the model parameters are investigated in terms of their physical relevance to breast tissue pathology information as well as their potential of breast cancer classification. The obtained results shows that our proposed dielectric model can excellently fit experimental data in most cases, while the extracted parameters of this model have a Pearson correlation of about 75% with fat and tumor percentages of examined tissue samples. The potential parameters of the dielectric model for breast cancer classification are confirmed through positive outcomes of the statistical analysis including independent two-tailed t-test and receiver operator characteristics (ROC) analysis. Leave-one-out cross-validation (LOOCV) values with support vector machines (SVM) classifiers support combining the model parameters to improve the classification accuracy in THz imaging of breast cancer.

This paper has the following structure. Section II is to introduce the mixture model of breast tissue, propose the fitting algorithm to extract the parameters of the proposed models, describe the tested data and discuss on simulation results. Section III provides the statistical and classification analysis of the extracted model parameters. Eventually, we summarize our contributions in Section IV.

II. DIELECTRIC PROPERTIES MODELING

A. Dielectric Model of Human Breast Tissue

Human tissue is commonly considered as a dispersive material whose dielectric properties including relative permittivity and conductivity depend on frequency. The increase of frequency leads to a remarkable decrease in the relative permittivity but conversely causes an upturn in conductivity. Complex permittivity of human tissue in a very low frequency range is well-described by the single-Debye relaxation model, while its responses in higher frequencies above 0.1 THz require extra Debye relaxation processes [11]

$$\epsilon = \epsilon_\infty + \sum_{n=1}^{N} \frac{\Delta\epsilon_n}{1 + \jmath\omega\tau_n} \qquad (1)$$

where $\Delta\epsilon_n$ indicates the permittivity dispersion of the nth-Debye relaxation process. The underlined fact of the multiple-Debye model is the higher water content of various human tissues [12], [13]. The double-Debye model was initially used as a dielectric function of water, and then, has inspired a significant number of applications for highly hydrated mixtures [7], [9], [14], [15]. For instance, the complex permittivity of human skin, which contains around 70% of water, has been accurately predicted by the two Debye relaxation processes [16], [17]. Muscle with higher water content than skin employs the summation of five Debye dispersions in addition to a frequency-dependent

conductivity term [18]

$$\epsilon = \epsilon_\infty + \sum_{n=1}^{5} \frac{\Delta\epsilon_n}{1 + \jmath\omega\tau_n} + \frac{\sigma}{\jmath\omega\epsilon_0}. \qquad (2)$$

However, dielectric properties of biological tissues with low water content and more complicated structure and composition exhibit broader dispersion that may involve superposition of several relaxation processes or non-first-order kinematics of molecular structure. The broadening of the dispersion could be resolved by adding a distribution parameter, and thus, the Cole–Cole (CC) equation has been introduced as an alternative of the Debye equation [13]. Eventually, the experimental dielectric spectra of various human tissues may be effectively described by multiple CC relaxation model [13], [19], [20] as

$$\epsilon = \epsilon_\infty + \sum_{n=1}^{N} \frac{\Delta\epsilon_n}{1 + (\jmath\omega\tau_n)^{1-\alpha_n}} + \frac{\sigma}{\jmath\omega\epsilon_0} \qquad (3)$$

where α_n is the distribution parameter measuring the broadening of the dispersion nth. The nonexponential relaxation processes described by the CC equation constitute a special case of non-Debye dielectric relaxation. The Havriliak–Negami (HN) relationship generalizes modeling the non-Debye relaxation processes by introducing two empirical exponents α and β [21]

$$\tilde{\epsilon}(\omega) = \epsilon_\infty + \frac{\epsilon_s - \epsilon_\infty}{[1 + (\jmath\omega\tau)^\alpha]^\beta}. \qquad (4)$$

In this regard, human breast is also composed of inhomogeneous structures of fat cells and proteins. The fatty (adipose) tissues have a low water content, and therefore, play a substantial role in regulating the dielectric responses of breast tissue. Indeed, the spectra of real permittivity of breast tissue increase at the low frequencies and pose quite a flat response over the higher frequency range, which is similar to that of pure adipose tissue. Particularly, Fig. 1 presents the average measured complex permittivities versus the frequencies for breast tumor, healthy fibrous breast tissue (fibrous), and healthy adipose tissue (fat), which were published by [8]. The error bars show the standard errors of the mean values with 95% confidence interval. Further details of the data are thoroughly described in Section II-C. Accordingly, while the most noticeable feature in dielectric properties of the breast tissues is the peak at around 0.32 THz, a similar increase is also spotted at 0.5 THz in dielectric spectrum of fat tissue. The physical origin of this dielectric response is yet to be understood [8], [22]. Therefore, we consider the increase of permittivity of breast tissue in the low range of THz regime as a non-Debye response. Apart from this, breast tissue still contains a relative-high proportion of water, which is the most prevalent source of absorption in THz frequencies, and thus, its complex permittivity like that of human skin may be also contributed by dielectric properties of water. In fact, the increase of THz frequency results in greater contribution of water absorption, thus the Debye relaxation process may be more transparent in the range above 1 THz. Considering the two aforementioned factors driving the dielectric spectra of breast tissue, we propose the following empirical mixture model based
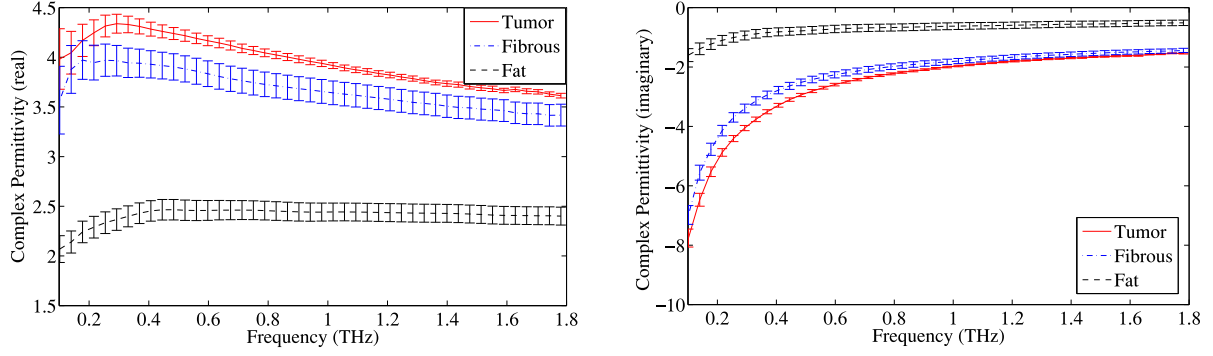
Fig. 1. Average complex permittivities with the corresponding error bars representing 95% confidence intervals for breast tumor, healthy fibrous breast tissue, and healthy fat (adipose) breast tissue from [8].

on a combination of non-Debye and Debye relaxation processes

$$\tilde{\epsilon}(\omega) = \boldsymbol{\epsilon}_\infty + \frac{\omega\boldsymbol{\tau}_1\boldsymbol{\Delta\epsilon}_1 + \boldsymbol{\Delta\epsilon}_2}{1 + (\jmath\omega\boldsymbol{\tau}_1)^{\boldsymbol{\alpha}}} + \frac{\boldsymbol{\Delta\epsilon}_3}{1 + \jmath\omega\boldsymbol{\tau}_2} + \frac{\boldsymbol{\sigma}}{\jmath\omega}. \quad (5)$$

Here, the term $(\omega\boldsymbol{\tau}_1\boldsymbol{\Delta\epsilon}_1 + \boldsymbol{\Delta\epsilon}_2)$ produces the peak in the real part of the complex permittivity of breast tissue at frequencies below 1 THz. $\boldsymbol{\Delta\epsilon}_1$ and $\boldsymbol{\Delta\epsilon}_2$ underline the existence of two dielectric dispersions occurring in the slow relaxation process characterized by time constant $\boldsymbol{\tau}_1$. However, it is important to emphasize that proposing these two parameters is more empirical rather than underlying any physical process, and thus, they should be simply regarded as necessary parameters to provide accurate fits. The dispersive amplitude of fast relaxation mode with the time constant $\boldsymbol{\tau}_2$ is $\boldsymbol{\epsilon}_3$ corresponding to high frequency. $\boldsymbol{\epsilon}_\infty$ is the limiting permittivity constant at very high frequency. $\boldsymbol{\sigma}/\jmath\omega$ represents the impact of dc-conductivity on dielectric loss of tissue.

As the real and imaginary part of the complex permittivity have different impacts on the values of the introduced parameters in (5), the significance of the difference in these two features between healthy breast tissues and tumor can suggest the cancer discrimination potential of the model parameters. Therefore, the normalized differences in the real and imaginary part of the average complex permittivities between tumor and healthy tissues, both fibrous and fat, were calculated and plotted over the examined frequency range in Fig. 2. Accordingly, the variation of the imaginary part of the complex permittivity between the healthy and cancerous tissues is more significant than that of the real part in most of the spectral range. The fact that only σ is fully driven by the dielectric loss marks this parameter as the most prevalent indicator of breast cancer among the parameters of the model (5). The theoretical assessment will be statistically investigated in depth in Section III-A.

B. Fitting Algorithm

In order to fit the data and extract the proper parameters of (5), we employ the sum of squared error functions (SSE), which calculate the differences between the measured frequency-dependent complex permittivities and their predicted values by one of these models over a range of consecutive THz frequencies.
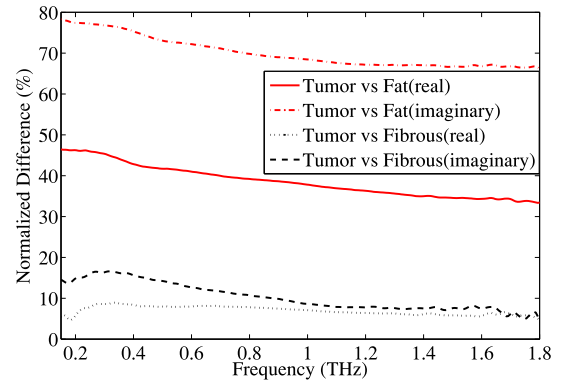

Fig. 2. Normalized percentage difference in the average complex permittivities between the two healthy breast tissue groups (fibrous and fat) and breast tumor.

Set $\boldsymbol{y} = (\boldsymbol{\epsilon}_\infty, \boldsymbol{\Delta\epsilon}_1, \boldsymbol{\Delta\epsilon}_2, \boldsymbol{\Delta\epsilon}_3, \boldsymbol{\sigma})^T = (\boldsymbol{y}_1, \boldsymbol{y}_2, \boldsymbol{y}_3, \boldsymbol{y}_4, \boldsymbol{y}_5)^T$. The optimization problem in order to fit the measured data is the following nonlinear least square

$$\min_{\boldsymbol{y},\,\boldsymbol{\tau}_1,\,\boldsymbol{\tau}_2,\,\boldsymbol{\alpha}} \quad \sum_{i=1}^{M} |\tilde{\epsilon}(\omega_i) - \tilde{\epsilon}_m(\omega_i)|^2$$

$$\text{subject to} \quad \boldsymbol{y}_1 \geq 1, \boldsymbol{y}_2 \geq 0, \boldsymbol{y}_3 \leq 0, \boldsymbol{y}_4 \geq 0, \boldsymbol{y}_5 \geq 0$$

$$\boldsymbol{y}_1 + \boldsymbol{y}_3 + \boldsymbol{y}_4 \geq 1$$

$$0.5 \leq \boldsymbol{\tau}_1,\, 0 \leq \boldsymbol{\tau}_2 \leq 0.5,\, \boldsymbol{\alpha} \geq 0 \quad (6)$$

where $\tilde{\epsilon}(\omega_i)$ defined by (5) is a highly nonlinear function of 8-D variable $(\boldsymbol{y}, \boldsymbol{\tau}_1, \boldsymbol{\tau}_2, \boldsymbol{\alpha})$, while $\tilde{\epsilon}_m(\omega_i)$ stands for the measured complex permittivity at a frequency ω_i. M is the number of sampling frequencies. The constraints of the model parameters in (6) are chosen to maintain the necessary physics properties of the complex dielectric model.

The problem (6) is seen as a very challenging optimization problem, for which the standard optimization tools and software are hardly suitable. Our first step is to analyze partially convex structures of (6) that are useful for computational purpose. It is seen from (5) that the objective function in (6) is convex quadratic in $\boldsymbol{y}$ when the three variables $\boldsymbol{\tau}_1, \boldsymbol{\tau}_2, \boldsymbol{\alpha}$ are held fixed. Thus, by setting $\boldsymbol{x} = (\boldsymbol{x}_1, \boldsymbol{x}_2, \boldsymbol{x}_3) = (\boldsymbol{\tau}_1, \boldsymbol{\tau}_2, \boldsymbol{\alpha})$, we reexpress

the total SSE in (6) by

$$f(\boldsymbol{x}, \boldsymbol{y}) = \boldsymbol{y}^T \sum_{i=1}^{M} A_i(\boldsymbol{x})\boldsymbol{y} + \sum_{i=1}^{M} b_i^T(\boldsymbol{x})\boldsymbol{y} + \sum_{i=1}^{M} d_i \quad (7)$$

where

$$A_i(\boldsymbol{x}) = a_i^*(\boldsymbol{x})a_i^T(\boldsymbol{x}), \; b_i^T = -2Re(c_i a_i^H), d_i = |\tilde{\epsilon}_m(\omega_i)|^2$$

$$A(\boldsymbol{x}) = \sum_{i=1}^{M} A_i(\boldsymbol{x}), b^T(\boldsymbol{x}) = \sum_{i=1}^{M} b_i^T(\boldsymbol{x}), d = \sum_{i=1}^{M} d_i$$

$$a_i(\boldsymbol{x}) = \left[1, \frac{\omega_i \boldsymbol{\tau}_1}{1 + (\jmath\omega_i \boldsymbol{\tau}_1)^{\boldsymbol{\alpha}}}, \frac{-1}{1 + (\jmath\omega_i \boldsymbol{\tau}_1)^{\boldsymbol{\alpha}}}, \frac{1}{1 + \jmath\omega_i \boldsymbol{\tau}_2}, \frac{1}{\jmath\omega_i} \right]^T.$$

Eventually, instead of the optimization problem (6) in eight decision variables, we consider the following optimization in 3-D variable $\boldsymbol{x}$:

$$\min_{\boldsymbol{x} \in X} F(\boldsymbol{x}) \quad (8)$$

with

$$F(\boldsymbol{x}) = \min_{\boldsymbol{y} \in Y} f(\boldsymbol{x}, \boldsymbol{y}). \quad (9)$$

Here, X and Y are linear constraints of $\boldsymbol{x}$ and $\boldsymbol{y}$, respectively, defined from (6) as

$$X = \{\boldsymbol{x} \in R^3 : 0.5 \le \boldsymbol{x}_1, \; 0 \le \boldsymbol{x}_2 \le 0.5, \; \boldsymbol{x}_3 \ge 0\}$$

and

$$Y = \{\boldsymbol{y} \in R^5 : \; \boldsymbol{y}_1 \ge 1, \boldsymbol{y}_2 \ge 0, \boldsymbol{y}_3 \le 0, \boldsymbol{y}_4 \ge 0$$
$$\boldsymbol{y}_5 \ge 0, \boldsymbol{y}_1 + \boldsymbol{y}_3 + \boldsymbol{y}_4 \ge 1\}.$$

It is simple to calculate each value $F(\boldsymbol{x})$ by using any existing convex quadratic solver such as SeduMi [23]. However, $F(\boldsymbol{x})$ is a 3-D nonconvex and nonsmooth function in the sense that almost everywhere there is only single $y(x) \in Y$ such that

$$f(x, y(x)) = F(x) \Leftrightarrow y(x) = \arg\min_{\boldsymbol{y} \in Y} f(x, y) \quad (10)$$

for which

$$\nabla F(x) = \frac{\partial f(x, y)}{\partial x}\Big|_{y=y(x)}. \quad (11)$$

For solution of (8), we will employ the robust gradient sampling algorithm [24]. The beforehand selected parameters are as follows.

1) Backtracking reduction factor $0 < \gamma < 1$. We choose $\gamma = 0.5$.
2) Armijo parameter in line search $0 < \beta < 1$. However, we choose a very small value of the Armijo parameter, which is practically equivalent to its nonstandard choice of 0.
3) Sampling size $m > \dim(x) = 3$. Thus, we set this parameter to $m = 7$.
4) Optimality tolerance reduction factor $\theta = 1$.
5) Sampling radius reduction factor $\mu = 0.5$.
   Initial parameters that will be iteratively updated are
1) Sampling radius ratio $\epsilon_0 = 0.1$.
2) Optimality tolerance $\nu_0 \ge 0$ is fixed to 10^{-6} throughout.
Iterations initialized from $x^{(0)} \in X$. For $\kappa = 0, 1, \ldots$.

1) *Step 1 (gradient sampling):* Take $u^{(\kappa_1)}, \ldots, u^{(\kappa_m)}$ sampled uniformly from the unit ball $\{u \in R^3 : ||u|| \le 1\}$ such that

$$x^{(\kappa_0)} = x^{(\kappa)}$$
$$x^{(\kappa_j)} = x^{(\kappa)}(1 + \epsilon_\kappa u^{(\kappa_j)}) \in X, \; j = 1, 2, \ldots, m. \quad (12)$$

For each $x^{(\kappa_j)}$, solve the quadratic program (10) to find $y(x^{(\kappa_j)})$ and define the gradient $\nabla F(x^{(\kappa_j)})$ according to (11).

2) *Step 2 (direction search):* Solve the quadratic program

$$\min_{\tau_j, j=0,1,\ldots,m} ||\tau_j \nabla F(x^{(\kappa_j)})||^2 \; : \; \tau_j \ge 0, \sum_{j=0}^{m} \tau_j = 1 \quad (13)$$

to have its optimal solution τ_j for the direction definition

$$g^{(\kappa)} = -\sum_{j=0}^{m} \tau_j \nabla F(x^{(\kappa_j)}). \quad (14)$$

If $||g^{(\kappa)}|| = 0$ stop ($x^{(\kappa)}$ is the optimal solution). If $||g^{(\kappa)}|| \le \nu_0$, set $t_\kappa = 0$, set the sampling radius $\epsilon_{\kappa+1} = \mu\epsilon_\kappa$, and go to Step 4. Otherwise keep $\epsilon_{\kappa+1} = \epsilon_\kappa$ and $d^{(\kappa)} = -g^{(\kappa)}/||g^{(\kappa)}||$ (normalized direction for line search), and go to Step 3.

3) *Step 3 (step length):* Use enumeration to solve

$$t_\kappa = \max_{s=0,1,2,\ldots} \gamma^s :$$
$$F(x^{(\kappa)} + \gamma^s d^{(\kappa)}) < F(x^{(\kappa)}) - \beta\gamma^s ||g^{(\kappa)}|| \quad (15)$$

(it is finite according to Armijo rule) and go to Step 4.

4) *Step 4 (update):* Set

$$x^{(\kappa+1)} = x^{(\kappa)} + t_\kappa d^{(\kappa)} \quad (16)$$

and $\kappa + 1 = \kappa$. Go to Step 1.

C. Simulation Data

Refractive indices and absorption coefficients of 74 breast samples are used to test the validity of the proposed model (5). The data were presented with group average values and error bars in [8]. Measurement procedures using THz spectroscopy in transmission geometry were also fully described by [8]. In brief, breast specimens were excised from 20 nonconsecutive female patients and preserved in refrigerated and humid condition. A THz time-domain spectrometer (TPIspectra1000, TeraView Ltd, Cambridge, U.K.) was used to measure the transmitted THz pulses through the tissue samples prepared from the patient specimens. The THz properties of the samples were calculated by averaging the measured refractive indices and absorption coefficients. The percentage content of fat (healthy adipose tissue), fibrous (healthy fibrous tissue), and cancer/tumor for each sample was determined by a Consultant Breast Pathologist and this served as a true reference to evaluate the THz data. Then, each of these samples was categorized according to its predominant constituent, which occupied more than 50% of the whole tissue.

TABLE I
EXTRACTED PARAMETERS OF THE MODEL (5) BY FITTING FOR HUMAN BREAST TISSUES

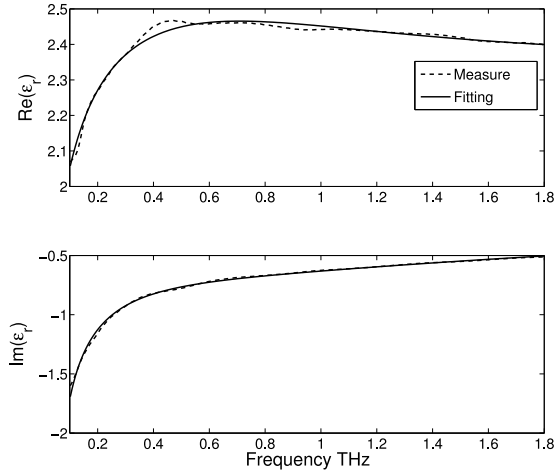| Sample	ϵ_∞	$\Delta\epsilon_1$	$\Delta\epsilon_2$	$\Delta\epsilon_3$	σ	τ_1 (ps)	τ_2 (ps)	α	SSE	aR^2
Adipose	2.50	3.54	−1.89	0.47	0.39	9.67	0.13	1.49	0.06	0.996
Normal	3.34	1.33	−3.05	0.71	5.27	1.91	0.11	1.20	0.41	0.998
BCC	2.86	28.64	−3.45	1.59	8.33	3.58	0.10	2.91	1.09	0.997

Fig. 3. Measured average complex permittivities of healthy fat tissue from [8] and its fitting by model.
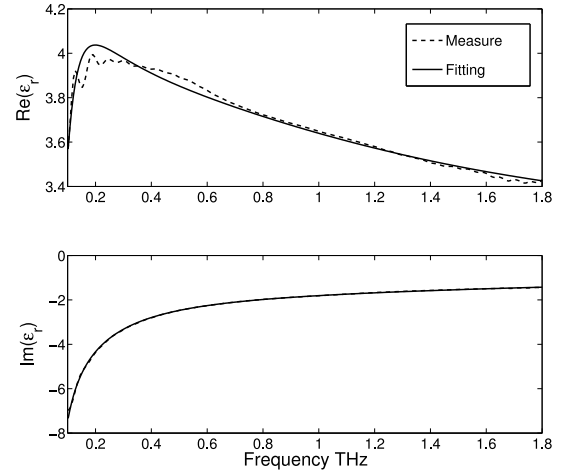

Fig. 4. Measured complex permittivities of healthy fibrous breast tissue from [8] and its fitting by model.

Complex permittivities calculated from these spectra represent the standard dielectric response of fat, fibrous tissue, and tumor of human breast to THz radiation. More details of the calculations to obtain the data were thoroughly provided in [8].

D. Fitting Results

In this section, the capability of the model (5) to simulate the complex permittivity of human breast tissue is investigated through fitting this model to the data of pure adipose tissue, fibrous tissue, and tumor. We employ the adjusted R-square value (aR^2), which is the square of the correlation between the response values and the predicted response values, to analyze the fitting quality [25]. It can be seen in Table I that the adjust R-squares in all three cases achieve the overall value from 0.99. Figs. 3, 4 and 5 demonstrate the comparison between complex permittivity simulated by (5) and the measured data for healthy breast tissue and breast tumor, respectively. The proposed dielectric model (5) mimics very well the dielectric properties of breast tissue not only at the high range of frequency beyond 1 THz but also at the lower frequencies. It is worth emphasizing that the non-Debye response of the real part of the breast tissue complex permittivity can be characterized well by (5). This advance of the model (5) is practically essential for breast cancer detection as the maximum difference between healthy and cancerous tissue in optical properties was found at the low spectral range, especially 0.32 THz [8]. The fitting parameters of (5) and aR^2s for healthy tissue and tumor are recorded in Table II. Accordingly, the contrast values in the model parameters of (5) between healthy and cancerous tissue suggest the
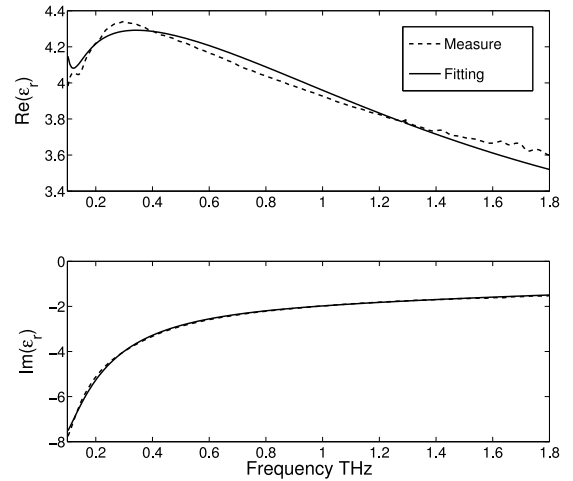

Fig. 5. Measured complex permittivities of breast tumor from [8] and its fitting by model.

potential of treating these parameters as indicators to classify the breast tumors.

The fitting parameters of (5) and aR^2s for all samples are recorded in groups of fat, fibrous, and tumor with their average values (AVR) and corresponding standard errors (SE) in Table II. According to the statistical values of aR^2, the model (5) can simulate the measured complex permittivities of fibrous tissue and tumor better than those of fat tissue. This may be explained by the higher water content of the former, especially tumor. In fact, since THz radiation is very sensitive to water, the dielectric properties of tumor and fiber possess less nonsmooth responses and noise both of which can negative impact on the predictability

TABLE II
GROUP AVERAGE OF THE EXTRACTED PARAMETERS WITH THEIR
STANDARD ERRORS AND THE CORRESPONDING AVERAGE aR^2
OF THE FITTINGS FOR ALL 74 DATA SAMPLES FROM [8]

Parameter	Fat	Fibrous	Tumor
ϵ_∞	2.41 ± 0.20	2.80 ± 0.31	3.15 ± 0.13
$\Delta\epsilon_1$	2.69 ± 2.15	38.22 ± 33.14	545.60 ± 980.60
$\Delta\epsilon_2$	-1.12 ± 0.56	-2.47 ± 0.67	-2.82 ± 0.43
$\Delta\epsilon_3$	0.61 ± 0.26	1.31 ± 0.25	1.34 ± 0.13
σ	1.12 ± 0.27	4.41 ± 0.88	7.89 ± 0.71
τ_1 (ps)	2.07 ± 0.61	3.50 ± 1.50	4.69 ± 4.25
τ_2 (ps)	0.12 ± 0.03	0.14 ± 0.04	0.10 ± 0.01
α	1.67 ± 0.30	1.91 ± 0.37	1.90 ± 0.28

of the model (5). In general, the AVRs of ϵ_∞, $\Delta\epsilon_1$, $\Delta\epsilon_3$, τ_1, τ_2, α are not apparently different between breast tissue types, while the large SEs of these parameters reveal the high possibility of overlaps of their values between tissue groups. On the contrary, $\Delta\epsilon_2$ and σ have obvious different AVRs between dominantly fat, fibrous, and tumor tissues, while their SE are rather small in comparison to these differences. This suggests $\Delta\epsilon_2$ and σ to be essential signatures of breast cancer applications, especially the cancer margin detection in THz imaging. An analysis in terms of the classification potential of the model parameters is exposed in the next section.

III. PARAMETERS SENSITIVITY ANALYSIS

All 74 human breast samples are fitted by the model (5) using the described gradient sampling algorithm. The average value of each model parameter and its standard error in each breast tissue group is tabulated in Table II. The contrast values in these parameters between tissue groups suggest their possible application for breast cancer classification. In the following sections, we shall employ essential statistical measures to analyze the differences offered by these model parameters, and accordingly select potential parameters for breast cancer classification.

A. Statistics Analysis

Pearson correlations between the model parameters and tissue histopathology are presented in Table III. The parameter σ of the mixture model (5) provide the highest correlation -0.75 with the fat percentage of tissue. This negative value of correlation implies that the reduction in the value of σ is proportional to the increase of fat percentage in the examined samples. Alternately, the correlation 0.75 of σ with tumor content explains the contribution of increasing neoplasm to the rise of this parameter. In fact, the similarity between fat and tumor in terms of high correlation with σ represents the nature that tumor has less adipose tissue and a more homogeneous structure in that respect as compared to fibrous tissue. One of the recent challenges in breast cancer detection with THz imaging is that the dielectric properties/optical properties of fibrous tissue and tumor are similar [8]. In fact, fibrous tissue together with glands and connective duct have a high water content and hence respond to THz radiation as comparably as cancerous tissue does [26]. As a result, it is clinically more apparent to detect tumors buried

in fatty tissues rather than those in fibrous tissues. However, tumor is still expected to contain more water (up to 20% higher) than fibrous tissue, which could be essential for distinguishing between these two types of tissues. In addition, the similarity between fat and tumor in terms of high correlation with σ represents the nature that tumor has less adipose tissue and a more homogeneous structure in that respect as compared to fibrous tissue. Indeed, the significantly higher average value 7.89 of σ for tumors than the value 4.41 of fibrous tissue can be found in Table II. In short, σ marks itself a highly prominent feature for differentiating tumor from fibrous tissue. Despite that we could not find the correlation between fibrous percentage and the parameters of model (5), it is worth reminding that Pearson correlation only measures the linear relationship between two variables. Therefore, the relationship between the model parameters and fibrous content may be nonlinear and Pearson correlation is probably not a suitable statistical measure for such a case.

As the Pearson correlation is to reveal the physical meaning behind the values of model parameters rather than to directly analyze the contrast between tissue group, we employ the independent two-tailed t-test with eight parameters of the mixture model. The specific p-values of the test corresponding to each pair of healthy tissue and tumor were provided in Table IV. The parameter σ demonstrates the statistically significant difference between fibrous tissue and tumor with the p-value of approximately 0, which is considerably lower than the critical value 0.05 of the t-test. Similar statistical results are also seen between fat and tumor. While ϵ_∞, $\Delta\epsilon_2$, $\Delta\epsilon_3$, σ, τ_1, τ_2 can demonstrate significant differences between healthy breast tissue and tumor, only ϵ_∞, σ is capable of specifying the difference between fibrous tissue and tumor.

B. Classification Potential

Both the Pearson correlation analysis and independent two-tailed sample t-test introduce the two parameters $\Delta\epsilon_3$ and σ of (5) as an advantageous indicator, which is highly sensitive to histopathology of breast samples. Therefore, an analysis from the perspective of classification is essential to accurately select rich features as well as confirm the potential of our model-parameter approach in breast cancer margin detection with THz imaging. A common technique to explore the sensitivity and specificity of classifiers in medical community is the ROC plot [27]. The ROC plots present the tradeoffs between the true positive rate (TPR) and the false positive rate (FPR), which is determined by one minus the specificity. Each operating point of the plot is identified by a pair of TPR and FPR corresponding to a threshold of the examined classifier. Fig. 6 demonstrates the ROC plot for σ as a classifier with its threshold values chosen by averaging two consecutive test values of σ. For the purpose of evaluating σ regarding its merit of classification, another critical index from ROC plots is the area under the ROC curve (AUROC), which is independent from any specific threshold and the most useful to generally assess the performance of a classifier. A value of AUROC close to 1 illustrates that its corresponding diagnosis system has higher sensitivity and specificity. The AUROC values of all eight model parameters were

TABLE III
PEARSON CORRELATION BETWEEN THE PARAMETERS OF THE MODEL (5) AND THE PERCENTAGE OF TISSUE COMPONENTS

Component	ϵ_∞	$\Delta\epsilon_1$	$\Delta\epsilon_2$	$\Delta\epsilon_3$	σ	τ_1 (ps)	τ_2 (ps)	α
Fat	−0.50	−0.09	−0.50	−0.61	−0.75	−0.122	−0.01	−0.09
Fiber tissue	−0.01	−0.05	0.14	0.25	−0.17	0.02	0.29	−0.16
Tumor	0.42	0.11	0.29	0.30	0.75	0.09	−0.21	0.08

TABLE IV
P-VALUE OF INDEPENDENT TWO-TAILED SAMPLE t-TEST FOR EACH PAIR OF SAMPLE GROUPS

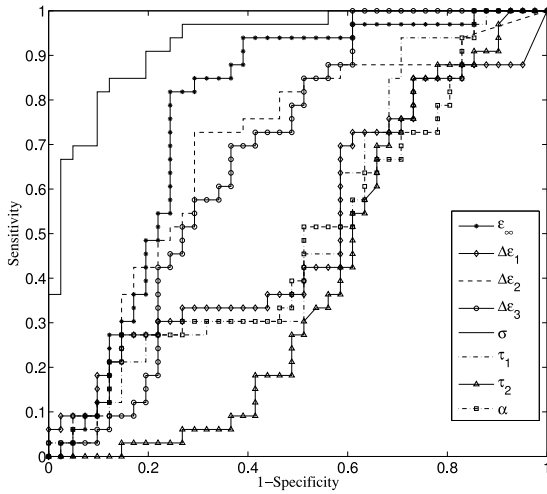| Pair of groups	ϵ_∞	$\Delta\epsilon_1$	$\Delta\epsilon_2$	$\Delta\epsilon_3$	σ	τ_1 (ps)	τ_2 (ps)	α
Fat tissue versus Tumor	1.92E-6	0.29	4.16E-5	3.75E-5	3.88E-20	0.25	0.27	0.28
Fibrous tissue versus Tumor	0.05	0.33	0.4	0.84	4.64E-7	0.61	0.08	1.00
Normal Tissue versus Tumor	6.12E-5	0.31	0.00	0.01	1.75E-14	0.42	0.04	0.58

Fig. 6.   ROC plot for various thresholds of σ.

TABLE V
AUROC VALUES OBTAINED BY ROC OF EACH MODEL PARAMETER OF (5)

ϵ_∞	$\Delta\epsilon_1$	$\Delta\epsilon_2$	$\Delta\epsilon_3$	σ	τ_1 (ps)	τ_2 (ps)	α
0.77	0.51	0.69	0.67	0.93	0.52	0.40	0.50

calculated and recorded in Table V. Particularly, the AUROC of σ is the highest with the value of 0.93. To the best of our knowledge, this outcome is remarkably higher than the best AUROC value of up to 0.78 in the literature [28]. Therefore, σ is selected to be the principal classification feature. The remaining parameters of the model (5) can be considered as supporting features to improve the classification capability. However, combination of well-correlated parameters do not facilitate improvement of classification capability, thus it is necessary to find the independence parameters for the combination. As a result, linear correlations between all eight model parameters were calculated to determine the independent parameters for classification.

In order to analyze the true classification power of σ and its combinations, internal or training error rates of these features

with SVM classifiers are employed. One way to estimate the true error rate is cross validation (CV), which is based on the idea of repeatedly training a model with a preselected proportion of data and testing the error rate of the model on the rest of the data [29]. For the well-known k-fold CV, the data are divided into k disjoint sets of which each consecutive set is used for testing the model trained by the remaining partition [30]. The k-CV value is calculated by averaging the correct classification accuracy over k training-testing times. Due to the small sample size in this study, LOOCV, the most complicated form of the k-fold CV, is applied to estimate the true error rate. Indeed, LOOCV allows using the most of data for training and can provide an unbiased error rate [31]. The SVM classifiers are applied for the model parameters and their combinations to determine the LOOCV values of all these features. The SVM algorithm aims to detect the decision boundaries between classes in the reduced dimension feature spaces. This method finds the optimal separating hyperplane with maximal margin between the classes by iteratively minimizing the objective function of the distance between support vectors of the classes. In this study, we employ the SVM classifiers with the MATLAB implementation developed by [32]. The kernel function, radial basic function used in our classification requires selecting the kernel parameter γ appropriately. In addition, the penalty parameter C of the error term in the objective function is also necessary for optimizing the classification. These two parameters are chosen by grid search to obtain the best LOOCV value. The LOOCV values of totally eight model parameters and their noticeable combinations are presented in Table VI. As expected, σ has the highest LOOCV accuracy of 86.49% among eight model parameters. Based on grouping the parameters, which are not statistically correlated, the best combination of these parameters is formed by ϵ_∞, $\Delta\epsilon_3$, σ with the LOOCV accuracy of up to 93.24%. In this respect, the significantly higher LOOCV accuracies of the combinations ϵ_∞, $\Delta\epsilon_3$, σ, and ϵ_∞, σ reveal their superior classification capability as compared to σ. In short, the outcomes of LOOCV analysis with the SVM classifier not only confirm the classification potential of σ but also explore the high feasibility of improving the accuracy with the combinations of the model parameters in (5) in THz imaging of breast cancer.

TABLE VI
SVM Classification Accuracy (%) in LOOCV Corresponding to Each Model Parameter and their Combinations

	ϵ_∞	$\Delta\epsilon_1$	$\Delta\epsilon_2$	$\Delta\epsilon_3$	σ	τ_1 (ps)	τ_2 (ps)	α	$(\epsilon_\infty, \sigma)$	$(\epsilon_\infty, \Delta\epsilon_3, \sigma)$
LOOCV (%)	81.08	68.92	74.32	63.51	86.49	67.57	63.51	63.51	91.89	93.24

IV. Conclusion

The mixed model for complex permittivity of breast tissue at THz frequencies as given in (5) is proposed for the first time. The dielectric model (5) is developed based on combining the non-Debye relaxation theory and the Debye relaxation process due to the nonexponential dielectric response of breast tissue at low THz frequencies and the impact of a considerable proportion of water in breast tissue. Our fitting procedure employed the gradient sampling algorithm for nonoptimization to extract optimal parameters of the model (5). Simulations prove that our proposed models can accurately mimic the measured data of fat/adipose tissue, healthy fibrous, and cancerous breast tissue. A variety of statistical measures were used to investigate the potential of the parameters of model (5) in terms of unveiling the tissue histopathology and cancer classification. Our analysis demonstrates two encouraging results: the parameter σ of (5) highly correlates with fat tissue and tumor percentage of examined breast tissue samples, which marks this parameter as an indicator for pathology diagnosis; the ROC analysis confirms the more remarkable discrimination ability of σ to classify breast cancer as compared to previous studies. In addition, LOOCV values of the combinations of the model parameters, namely $(\epsilon_\infty, \sigma)$ and $(\epsilon_\infty, \Delta\epsilon_3, \sigma)$, with the SVM classifier suggest these features as the best indicators for discriminating breast tumor from healthy breast tissue. To recapitulate, these outcomes support a further step toward understanding the dielectric responses of breast tissue to THz radiation as well as applying the parameters of model (5) into THz imaging for breast cancer detection.

Future study will consider direct classification on more THz images in order to confirm the accuracy of breast cancer margin detection. Moreover, the empirical model (5) also requires more specific elaboration on physical process underlying the non-Debye dielectric response of breast tissue in the future. Knowing the best way to describe the dielectric properties, we will be able to apply the finite-difference time-domain techniques using the proposed model to simulate the interaction of THz radiation with breast tissue. Therefore, we can recognize the theoretical differences in pulse shape between normal and tumor tissue as well as improve our understanding of how normal tissue changes its response due to tumorigenesis. This will be beneficial to deal with heterogeneous tissue, which includes both characteristics of tumor and normal. A THz intraoperative probe has been developed that can perform measurements in reflection geometry during breast cancer surgery; the outcomes of this study will facilitate choosing classification features in the pulse shape of the reflected signal collected using this probe. Furthermore, successfully modeling the dielectric response of breast tissue with the model (5) implies that the low THz frequency range is the most accountable for producing the data to classify breast cancer. Applying the low frequencies for a practical THz imaging system, mainly THz pulse imaging or single frequency THz Imaging, leads to a sacrifice in spatial resolution since the minimum size of tumor identifiable by THz needs to be larger. For instance, 1 THz generally has a spatial resolution of around 300 micrometer. Consequently, the application of THz imaging is limited to sampled areas larger than this size.

References

[1] A. J. Fitzgerald, S. Pinder, A. D. Purushotham, P. OKelly, P. C. Ashworth, and V. P. Wallace. (2012). Classification of terahertz-pulsed imaging data from excised breast tissue. *J. Biomed. Opt.* [Online]. *17(1)*, pp. 016 005-1–016 005-10. Available: http://dx.doi.org/10.1117/1.JBO.17.1.016005

[2] A. J. Fitzgerald, V. P. Wallace, M. Jimenez-Linan, L. Bobrow, R. J. Pye, A. D. Purushotham, and D. D. Arnone. (2006). Terahertz pulsed imaging of human breast tumors. *Radiology*. [Online]. *239(2)*, pp. 533–540. Available: http://radiology.rsna.org/content/239/2/533.abstract

[3] A. Hassan, D. Hufnagle, M. El-Shenawee, and G. Pacey, "Terahertz imaging for margin assessment of breast cancer tumors," in *Proc. IEEE MTT-S Int. Microw. Symp. Dig.*, Jun. 2012, pp. 1–3.

[4] E. Berry, G. C. Walker, A. J. Fitzgerald, N. N. Zinovev, M. Chamberlain, S. W. Smye, R. E. Miles, and M. A. Smith. (2003). Do *in vivo* terahertz imaging systems comply with safety guidelines?, *J. Laser Appl.* [Online]. *15(3)*, pp. 192–198. Available: http://scitation.aip.org/content/lia/journal/jla/15/3/10.2351/1.1585079

[5] V. P. Wallace, P. F. Taday, A. J. Fitzgerald, R. M. Woodward, J. Cluff, R. J. Pye, and D. D. Arnone, "Terahertz pulsed imaging and spectroscopy for biomedical and pharmaceutical applications," *Faraday Discussions*, vol. 126, pp. 255–263, 2004.

[6] R. M. Woodward, V. P. Wallace, R. J. Pye, B. E. Cole, D. D. Arnone, E. H. Linfield, and M. Pepper, "Terahertz pulse imaging of ex vivo basal cell carcinoma." *J. Investigative Dermatol.*, vol. 120, no. 1, pp. 72–78, 2003.

[7] S. W. Smye, J. M. Chamberlain, A. J. Fitzgerald, and E. Berry, "The interaction between terahertz radiation and biological tissue," *Phys. Med. Biol.*, vol. 46, no. 9, pp. R101–R112, 2001.

[8] P. C. Ashworth, E. Pickwell-MacPherson, E. Provenzano, S. E. Pinder, A. D. Purushotham, M. Pepper, and V. P. Wallace. (2009, Jul.). Terahertz pulsed spectroscopy of freshly excised human breast cancer. *Opt. Exp.* [Online]. *17(15)*, pp. 12 444–12 454. Available: http://www.opticsexpress.org/abstract.cfm?URI=oe-17-15-12444

[9] E. Pickwell, B. E. Cole, A. J. Fitzgerald, V. P. Wallace, and M. Pepper, "Simulation of terahertz pulse propagation in biological systems," *Appl. Phys. Lett.*, vol. 84, no. 12, pp. 2190–2192, 2004.

[10] A. J. Fitzgerald, E. Pickwell-MacPherson, and V. P. Wallace, "Use of finite difference time domain simulations and Debye theory for modelling the terahertz reflection response of normal and tumour breast tissue," *PLoS ONE*, vol. 9, no. 7, pp. e99291-1–e99291-9, 2014.

[11] H. Liebe, G. Hufford, and T. Manabe. (1991). A model for the complex permittivity of water at frequencies below 1 THz. *Int. J. Infrared Millimeter Waves*. [Online]. *12(7)*, pp. 659–675. Available: http://dx.doi.org/10.1007/BF01008897

[12] K. R. Foster and H. P. Schwan, "Dielectric properties of tissues and biological materials: A critical review." *Crit. Rev. Biomed. Eng.*, vol. 17, no. 1, p. 25, 1989.

[13] S. Gabriel, R. W. Lau, and C. Gabriel, "The dielectric properties of biological tissues: III. parametric models for the dielectric spectrum of tissues," *Phys. Med. Biol.*, vol. 41, no. 11, p. 2271, 1996.

[14] J. T. Kindt, and C. A. Schmuttenmaer, "Far-infrared dielectric properties of polar liquids probed by femtosecond terahertz pulse spectroscopy," *Jo. Phys. Chem.*, vol. 100, no. 24, pp. 10 373–10 379, 1996.

[15] C. B. Reid, E. Pickwell-MacPherson, J. G. Laufer, A. P. Gibson, J. C. Hebden, and V. P. Wallace. (2010). Accuracy and resolution of thz reflection spectroscopy for medical imaging. *Phys. Med. Biol.* [Online]. *55(16)*, p. 4825. Available: http://stacks.iop.org/0031-9155/55/i=16/a=013

[16] E. Pickwell, A. J. Fitzgerald, B. E. Cole, P. F. Taday, R. J. Pye, T. Ha, M. Pepper, and V. P. Wallace, "Simulating the response of terahertz radiation to basal cell carcinoma using ex vivo spectroscopy measurements," *J. Biomed. Opt.*, vol. 10, no. 6, pp. 064021-1–064021-7, 2005.

[17] B. C. Q. Truong, H. D. Tuan, H. H. Kha, and H. T. Nguyen, "Debye parameter extraction for characterizing interaction of terahertz radiation with human skin tissue," *IEEE Trans. Biomed. Eng.*, vol. 60, no. 6, pp. 1528–1537, June 2013.

[18] W. Hurt, "Multiterm debye dispersion relations for permittivity of muscle," *IEEE Trans. Biomed. Eng.*, vol. BME-32, no. 1, pp. 60–64, Jan. 1985.

[19] C. Gabriel, S. Gabriel, and E. Corthout, "The dielectric properties of biological tissues: I. Literature survey," *Phys. Med. Biol.*, vol. 41, no. 11, pp. 2231–2249, 1996.

[20] T. Said and V. Varadan, "Modeling the effective complex permittivity of heterogeneous breast tissue and comparison with relaxation models at millimeters wave frequencies," in *Proc. IEEE Region 5 Techn. Conf.*, 2007, pp. 157–162.

[21] S. Havriliak and S. Negami. (1967). A complex plane representation of dielectric and mechanical relaxation processes in some polymers. *Polymer*. [Online]. *8(0)*, pp. 161–210. Available: http://www.sciencedirect.com/science/article/pii/0032386167900213

[22] U. Khan, N. Al-Moayed, N. Nguyen, M. Obol, K. Korolev, M. Afsar, and S. Naber, "High frequency dielectric characteristics of tumorous and non-tumorous breast tissues," in *Proc. IEEE/MTT-S Int. Microw. Symp.*, June 2007, pp. 1341–1344.

[23] J. F. Sturm, "Using sedumi 1.02, a MATLAB toolbox for optimization over symmetric cones," *Optimization Methods Softw.*, vol. 11, no. 1, pp. 625–653, 1999.

[24] J. Burke, A. Lewis, and M. Overton. (2005). A robust gradient sampling algorithm for nonsmooth, nonconvex optimization. *SIAM J. Optimization*. [Online]. *15(3)*, pp. 751–779. Available: http://epubs.siam.org/doi/abs/10.1137/030601296

[25] MATLAB, *Curve Fitting Toolbox*. The MathWorks Inc., Natick, MA, USA, 2012.

[26] H. Chen, T. H. Chen, T. F. Tseng, J. T. Lu, C. C. Kuo, S. C. Fu, W. J. Lee, Y. F. Tsai, Y. Y. Huang, E. Y. Chuang, Y. J. Hwang, and C. K. Sun. (2011, Oct.). High-sensitivity *in vivo* thz transmission imaging of early human breast cancer in a subcutaneous xenograft mouse model. *Opt. Exp.* [Online]. *19(22)*, pp. 21 552–21 562. Available: http://www.opticsexpress.org/abstract.cfm?URI=oe-19-22-21552

[27] T. Fawcett, "Roc graphs: Notes and practical considerations for researchers," *ReCALL*, vol. 31, no. HPL-2003-4, pp. 1–38, 2004.

[28] B. St.Peter, S. Yngvesson, P. Siqueira, P. Kelly, A. Khan, S. Glick, and A. Karellas, "Development and testing of a single frequency terahertz imaging system for breast cancer detection," *IEEE Trans. Terahertz Sci. Technol.*, vol. 3, no. 4, pp. 374–386, Jul. 2013.

[29] L. D. Fisher, and G. van Belle, *Biostatistics: A Methodology for the Health Sciences*. Hoboken, NJ, USA: Wiley, 1993.

[30] R. Kohavi. (1995). A study of cross-validation and bootstrap for accuracy estimation and model selection. in *Proc. 14th Int. Joint Conf. Artif. Intell.*, San Francisco, CA, USA, pp. 1137–1143. [Online]. Available: http://dl.acm.org/citation.cfm?id=1643031.1643047

[31] G. C. Cawley and N. L. Talbot. (2003). Efficient leave-one-out cross-validation of kernel fisher discriminant classifiers. *Pattern Recog.* [Online]. *36(11)*, pp. 2585–2592. Available: http://www.sciencedirect.com/science/article/pii/S0031320303001365

[32] C. C. Chang and C. J. Lin. (2011). LIBSVM: A library for support vector machines. *ACM Trans. Intell. Syst. Technol.* [Online]. *2*, pp. 27-1–27-27. Available: http://www.csie.ntu.edu.tw/ cjlin/libsvm

Bao C. Q. Truong (S'12) received the B.E. degree in electrical and electronics engineering from Ho Chi Minh City University of Technology, Ho Chi Minh, Vietnam, in 2011. He is currently working toward the Ph.D. degree in biomedical engineering at University of Technology Sydney, Ultimo, Australia.

His current research interests include biomedical applications of optimization algorithm, machine learning algorithm, statistical analysis, terahertz technologies, and medical imaging.

Hoang D. Tuan (M'94) was born in Hanoi, Vietnam. He received the diploma and the Ph.D. degree in applied mathematics from Odessa State University, Odessa, Ukraine, in 1987 and 1991, respectively.

From 1991 to 1994, he was a Researcher with the Optimization and Systems Division, Vietnam National Center for Science and Technologies. He was an Assistant Professor in the Department of Electronic-Mechanical Engineering, Nagoya University, Nagoya, Japan, from 1994 to 1999 and an Associate Professor in the Department of Electrical and Computer Engineering, Toyota Technological Institute, Nagoya, from 1999 to 2003. He was a Professor in the School of Electrical Engineering and Telecommunications, the University of New South Wales, Sydney, Australia, from 2003 to 2011. He is currently a Professor of the Centre for Health Technologies, Faculty of Engineering and Information Technology, University of Technology Sydney Ultimo, Australia. His research interests include theoretical developments and applications of optimization based methods in many areas of control, signal processing, communication, and bioinformatics.

Anthony J. Fitzgerald received the B.Sc. degree from the University of Western Australia, Crawley, Australia, in 1990, and the Ph.D. degree in medical physics from the Queensland University of Technology, Brisbane, Australia, in 1997.

He has applied novel imaging methods to medical physics, including electrical impedance tomography (EIT) and terahertz pulsed imaging (TPI). His research interests include the terahertz pulsed spectroscopy of human biological tissues for medical applications and modeling the response and simulations of these tissues. Most recently he has focused on using TPI breast cancer imaging during surgery.

Vincent P. Wallace (M'03) received the Ph.D. degree in medical physics from the University of London, London, U.K., in 1997.

He has more than 18 years of experience in Biophotonics. After three years at the Beckman Laser Institute, UC Irvine, he joined Toshiba Research, Cambridge, U.K., to look at potential medical applications of terahertz radiation. TeraView Ltd., Cambridge, was spun-out of Toshiba Labs in April 2001. At TeraView, he led a group looking at medical applications of terahertz. In 2007, he moved to the University of Western Australia, where he continues to apply terahertz and other techniques to biomedical and clinical problems.

Hung T. Nguyen (SM'99) received the B.E. degree (with First Class and University Medal) and the Ph.D. degree from the University of Newcastle, Newcastle, Australia, in 1976 and 1980, respectively.

He is a Professor of electrical engineering at the University of Technology Sydney (UTS), Ultimo, Australia. He is the Dean of the Faculty of Engineering and Information Technology and the Director of the Centre for Health Technologies at the UTS. He has been involved with research in the areas of biomedical engineering, advanced control and artificial intelligence for more than 20 years. He has developed several biomedical devices and system for diabetes, disability, cardiovascular diseases, and breast cancer. He was an Engineering Manager of Power Electronics Pty Ltd., from 1988 to 1998, the Founding and Executive Director of AIMedics Pty Ltd., from 2001 to 2006, and the Associate Dean (Research and Development) in the Faculty, from 2003–2009.

Prof. Nguyen is a Fellow of the Institution of Engineers, Australia and The British Computer Society.